

1     **Ionospheric influence on the seismo-telluric current related to electromagnetic**  
2             **signals observed before the Wenchuan  $M_S=8.0$  earthquake**

3  
4                     Mei Li<sup>1,2</sup>, Handong Tan<sup>2</sup> and Meng Cao<sup>2</sup>

5  
6     (1) China Earthquake Networks Center, China Earthquake Administration, No.5,  
7             Sanlihe Nanhengjie, Xicheng District, 100045 Beijing, China.

8     (2) China University of Geosciences, No.29, Xueyuan Road, Haidian District, 100083  
9             Beijing, China.

10  
11     Corresponding author: Handong Tan, China University of Geosciences, No.29,  
12             Xueyuan Road, Haidian District, 100083 Beijing, China. (thd@cugb.edu.cn)

13  
14     **Abstract.** A three-layer (Earth-air-ionosphere) physical model, as well as a  
15 two-layer (Earth-air) model, is employed in this paper to investigate the ionospheric  
16 effect on the wave fields for a finite length dipole current source co-located **at a**  
17 **hypocenter depth and along** the main fault of an earthquake when the distance  
18 **between the epicenter and an observing station** is up to one thousand kilometers or  
19 even more. The results show that all electrical fields are free of ionospheric effect for  
20 different frequencies in a relative short range, e.g.,  $\sim 300$  km for  $f=1$  Hz, implying  
21 the ionospheric influence on electromagnetic fields can be neglected within this range,  
22 **which** becomes smaller as the frequency increases. However, the ionosphere can give  
23 a constructive interference to the waves passed through and make them decay slowly  
24 when an observation is out of this range and the ionospheric effect can be up to 1-2  
25 magnitudes of the electrical fields. For an observed  $1.3 \text{ mV m}^{-1}$  signal at 1,440 km  
26 away for the Wenchuan  $M_S=8.0$  earthquake, the expected seismo-telluric current  
27 magnitude for the Earth-air-ionosphere model is of  $5.0 \times 10^7 \text{ A}$ , one magnitude smaller  
28 than the current value of  $3.7 \times 10^8 \text{ A}$  obtained by the Earth-air model free of  
29 ionospheric effect. This indicates that the ionosphere facilitates the electromagnetic  
30 wave propagation, as if the detectability of the system is improved effectively and it is  
31 easier to record a signal even for stations located at distances beyond their  
32 detectability threshold. **Furthermore, the radiating patterns of the electrical field**  
33 **components  $|E_x|$  and  $|E_y|$  are complementary each other although anyone 2-D power**  
34 **distribution of them shows strong power areas as well as weak ones, which is**

35 advantageous to register a signal if the observing system is designed to measure both  
36 of them instead of only one.

37

38 **Keywords.** Ionospheric influence on electromagnetic waves; The Wenchuan  
39 earthquake; Seismo-telluric current; 2-D power distribution

40

## 41 **1 Introduction**

42 The fact that Electro-Magnetic (EM) emissions accompany every stage of large  
43 earthquake preparations seems undebatable although short-term earthquake prediction  
44 is still one of the most challenging targets in Earth science today (Eftaxias et al.,  
45 (2002). Meanwhile, the Ultra-Low Frequency (ULF) band is of particular interest  
46 because only EM signals in the ULF range and at lower frequencies originated in the  
47 Earth's crust can be easily recorded at the Earth's surface without significant  
48 attenuation comparing with 'high' frequency emissions that might be emitted at  
49 epicenter depths at more than 10 km, even several hundreds of kilometers. Recently,  
50 ULF electromagnetic anomalous phenomena related to strong earthquakes have been  
51 investigated and reported in increasing numbers. Some notable examples include the  
52 Loma Prieta  $M_s=7.1$  earthquake on October 17, 1989 ( $f=0.01-10$  Hz,  $D=7$  km,  $A=1.5$   
53 nT) (Fraser-Smith et al., 1990; Bernardi et al., 1991), as well as the Spitak  $M_s=6.9$   
54 earthquake on December 7, 1988 ( $f=0.005-1$  Hz,  $D=200$  km,  $A=0.2$  nT) (Molchanov  
55 et al., 1992; Kopytenko et al., 1993). In addition, the geo-electric potential  
56 enhancement appeared 1–19 days before five of all six EQs with magnitude  $>5$  that  
57 occurred within 75 km in Japan and its duration and intensity were several minutes to  
58 1 h with an amplitude of  $0.01-0.02$  mV m<sup>-1</sup> (Uyeda et al., 2000). Qian *et al.* (2002)  
59 have reported the observation of ULF signals generated from Jiji earthquake of 21  
60 September 1999 in Taiwan and recorded at many stations at distances of 300–900 km  
61 in South East China. Similarly, Ohta *et al.* (2002) have reported the observation of  
62 ULF/ELF emissions generated from Taiwan earthquake of 21 September, 1999 and  
63 recorded at Nakatsugawa station in Japan at a distance of up to 2000 km.

64 A more notable example reported by Li et al. (2013) is the Wenchuan  $M_s=8.0$   
65 earthquake on May 12, 2008, a typical mid-crust, which resulted in great devastation  
66 and 69,000 deaths. This earthquake was preceded by more than one month of  
67 increasing anomalous ULF emissions with a climax starting on May 9, three days  
68 before the Wenchuan main shock ( $f=0.1-10$  Hz,  $D=1,440$  km,  $A=1.3$  mV m<sup>-1</sup>).

69 Many simulating rock-pressure experiments were carried out in order to  
70 understand the producing mechanism of the electromagnetic information associated  
71 with seismic activities. Laboratory experiments by *Qian et al.*, [1996; 2003] and *Hao*  
72 *et al.* [2003] present that, electromagnetic signals are always recorded when rock  
73 samples are subjected to dynamic stresses. Electromagnetic pulses of shorter-period  
74 appearing at the last stage of the experiment may be induced by instantaneous electric  
75 current of the accumulated charge during the stress acceleration.

76 Recently, the work of Freund et al. (Freund and Wengeler, 1982, Freund, 2002,  
77 2009, 2010; Freund and Sornette, 2007; Scoville et al., 2015) has gained a new insight  
78 into the production of current and electromagnetic signals in stressed rocks. As rocks  
79 upon stressing, stresses cause slight displacements of mineral grains in the rocks,  
80 which in turn lead to the activation of peroxy defects that preferentially sit on or  
81 across grain boundaries. The peroxy break-up leads to positive holes  $h^*$  and the  $h^*$  are  
82 able to flow from stressed to unstressed rock, traveling fast and far by way of a  
83 phonon-assisted electron hopping mechanism using energy levels at the upper edge of  
84 the valence band. A gabbro sample ( $30 \times 15 \times 10 \text{ cm}^3$ ) from Shanxi, China, was used in  
85 the test and a 55 nA current recorded about 2 seconds before failure, with the load  
86 being at about 30,000 lbs and the maximum spike reaches 450 nA when the main  
87 failure took place (Freund, 2009).

88 Up to now, no clear explanation has been given although several physical  
89 mechanisms have been proposed to interpret the generation of EM emissions and  
90 electrical currents observed either during seismic activity or in the laboratory  
91 experiments. These include the electrokinetic and magnetohydrodynamic,  
92 piezomagnetism, stress-induced variations in crustal conductivity, microfracturing,  
93 and so on (Draganov et al., 1991; Park, 1996; Fenoglio et al., 1995; Egbert, 2002;  
94 Simpson and Taflove, 2005).

95 Whatever the physical mechanism of electromagnetic generation is, it is well  
96 established that, during rock experiments conducted under laboratory conditions, a  
97 strong electrical current is produced when rocks are stressed, especially at the stage of  
98 the main rupture. So, like what Bortnik et al. (2010) wanted to know, what is the  
99 electrical current necessary to produce an observable magnetic signal on the ground,  
100 at a given distance from the epicenter and for an assumed ground conductivity? In  
101 their work, an infinitesimally short, horizontal dipole located at a hypocenter depth in  
102 the half-space (Earth) is used to estimate the magnitude of the seismo-telluric current

103 required for the “Alum Rock”  $M_W=5.6$  earthquake on October 31, 2007. The  
104 observable electromagnetic ground signals ( $f=1$  Hz,  $D=2$  km,  $A=30$  nT) and the  
105 results show that for an observed 30 nT pulse at 1 Hz, the expected seismo-telluric  
106 current magnitudes fall in the range  $\sim 10\text{--}100$  kA.

107 Unlike a parameter of the “Alum Rock”  $M_W=5.6$  earthquake ( $D=2$  km), the  
108 distance between the epicenter of the Wenchuan  $M_S=8.0$  earthquake and the observing  
109 station is  $D\sim 1,440$  km (Li et al., 2013), i.e. several times **larger** than the height of **the**  
110 **lower edge** of ionosphere ( $h\sim 85\text{--}100$  km) (Kuo et al., 2011; Cummer, 2000; Yamauchi  
111 et al., 2007). When we investigate electromagnetic emissions induced by an electrical  
112 current or a magnetic moment on the surface or beneath the Earth, the effect of the  
113 medium air, crustal as well as ionosphere should be taken into account because of  
114 these three media being of different conductivities and so we need to consider a  
115 lithosphere-atmosphere-ionosphere electromagnetic coupling. The ionosphere plays  
116 an important role in radio propagation at Extremely Low Frequency (ELF) and Very  
117 Low Frequency (VLF), the ground and the ionosphere are good electrical conductors  
118 and form a spherical Earth-ionosphere waveguide (Cummer, 2000). In addition, in the  
119 magneto-telluric (MT) method, widely used in petroleum **exploration** or **mining**, the  
120 ionospheric influence on electromagnetic (EM) fields should be considered when the  
121 distance between a large-scale and large-power fixed source and the receiver is up to  
122 one thousand kilometers. EM fields can be amplified in the ionosphere as it is shown  
123 when we use analytical solutions of Maxwell equations, as well as numerical ones of  
124 the “Earth-ionosphere” mode with a source **on the Earth’s surface or in the lower**  
125 **atmosphere** (Fu et al., 2012; Li et al., 2010a; Li et al., 2010b; Xu et al., 2012; Li et al.,  
126 2011). Therefore, comparing with an electromagnetic attenuation without ionospheric  
127 effect, the point is to evaluate the ionospheric influence on the electromagnetic  
128 propagation when the transmitter-receiver distance is up to one thousand kilometers  
129 or even more. Furthermore, the comparison between the observation distance  
130 ( $D=1,440$  km) and the length of the Wenchuan earthquake main rupture  $L\sim 150$  km  
131 (Zhang et al., 2009) indicates that the length of the dipole source is not negligible. So  
132 in this paper, **based on** the work of Key (2009), a three-layer (Earth-air-ionosphere)  
133 physical model, as well as a two-layer (Earth-air) model, containing a finite length  
134 dipole current source co-located along the fault and beneath the Earth is introduced in  
135 Sect. 2. For specified parameters, some simulation results of the dipole source with  
136 and without ionospheric effect are given in Sect. 3. In Sect.4, we define and limit our

137 assumed parameter values, present the results for the Wenchuan earthquake case.  
 138 Discussion and conclusions are given in Sect. 5 and Sect.6, respectively.

139

## 140 2 Description of the modeling methodology

141 In order to study the electromagnetic fields emitted by a long dipole current  
 142 source, the approach used here follows the magnetic vector potential formulation  
 143 described in Wait (1982) and developed by Key (2009), who generalized the  
 144 formulation to allow for multiple layers above the transmitter (in addition to multiple  
 145 layers below). He used exponential forms for the recursions rather than hyperbolic  
 146 functions in isotropic media, which consists of N layers of isotropic conductivity  $\sigma_i$   
 147 where  $i = 1, \dots, N$ , and which uses a right-handed coordinate system with the z axis  
 148 pointing down. Assuming a time-harmonic source with  $e^{-i\omega t}$  time dependence,  
 149 negligible magnetic permeability  $\mu$  variations, and angular frequencies  $\omega$  that are  
 150 low enough so that displacement currents can be neglected, Maxwell's equations are

$$151 \quad \nabla \times \mathbf{E} = i\omega\mathbf{B}, \quad (1)$$

152 and

$$153 \quad \nabla \times \mathbf{B} = \mu\sigma\mathbf{E} + \mu\mathbf{J}_s. \quad (2)$$

154 Expression  $\mathbf{J}_s = \mathbf{I}\delta(\mathbf{r} - \mathbf{r}_0)$  is the imposed electric dipole source at position  $\mathbf{r}_0$  with  
 155 vector moment  $\mathbf{I}$ , and here is restricted to an infinitesimal dipole with unit moment.

156

157

158

159

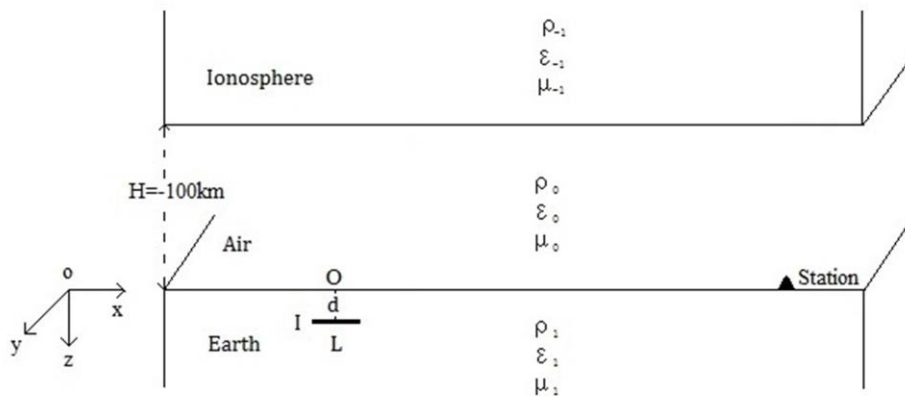
160

161

162

163

164



165

166 **Fig.1.** An x-directed dipole current source, with its central coordinate  $(0, 0, d)$ , is placed in the  
 167 bottom medium (Earth) of a three layer modeling (Earth-air-ionosphere model), where  $z$  is defined  
 168 positive in the downward direction.

169

170 Based on the model set up by Key (2009), some modifications will be done in

171 this study in order to answer the questions illustrated above. A physical model is  
172 specified. It has three layers, Earth, air and ionosphere, which is called  
173 Earth-air-ionosphere model. Its coordinate system is denoted in Fig.1 **with z-direction**  
174 **being downward**. An x-directed dipole of a length  $L$  and a current  $I$  is placed in the  
175 bottom medium (Earth:  $z > 0$ ), which is homogeneous and has the electrical  
176 properties: magnetic permeability  $\mu_1$ , permittivity  $\epsilon_1$ , and conductivity  $\sigma_1$ . The  
177 middle medium (air:  $-100 \text{ km} < z < 0$ ) is described by its electrical properties  $\mu_0$ ,  
178  $\epsilon_0 (= 8.854 \times 10^{-12} \text{ Farad m}^{-1})$  and  $\sigma_0 (= 10^{-14} \text{ S m}^{-1})$ . The top medium  
179 (ionosphere:  $z < -100 \text{ km}$ ) is characterized by electrical properties  $\mu_{-1}$ ,  $\epsilon_{-1}$  and  
180  $\sigma_{-1} (= 10^{-5} \text{ S m}^{-1})$ .

181 As a comparison, a two-layer model (Earth-air model) including in Earth  
182 medium ( $z > 0$ ), as well as air medium ( $z < 0$ ), is also established during the study.  
183 All the corresponding parameters described are the same as these of  
184 Earth-air-ionosphere model.

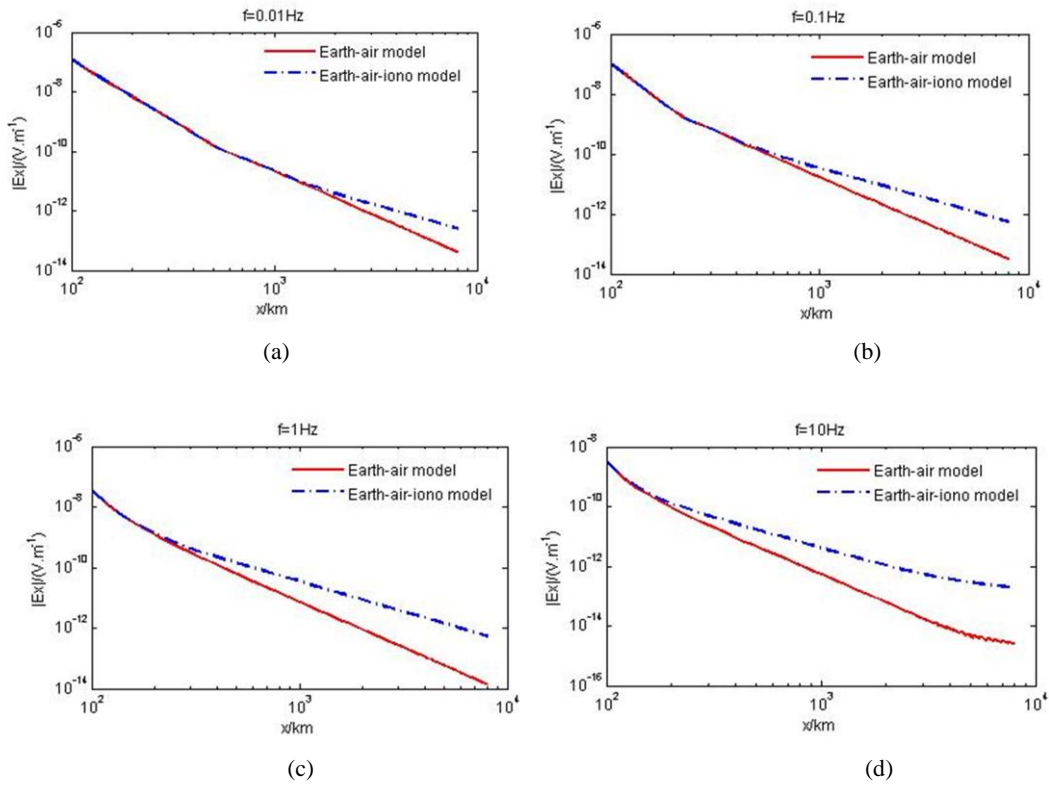
185 We assume that the total space is non-magnetic and that the magnetic  
186 permeability  $\mu$  variations are negligible in the different layers, i.e.  $\mu_1 = \mu_0 = \mu_{-1} =$   
187  $4\pi \times 10^{-7} \text{ Farad m}^{-1}$ . However, the ionosphere as the electrically conducting  
188 section of the upper atmosphere plays **such an important role for** the electromagnetic  
189 propagation that we set  $\epsilon_{-1} = 5\epsilon_0$  when an ionospheric effect on electromagnetic  
190 transmission is taken into consideration. On the same manner we have  $\epsilon_1 = \epsilon_0 =$   
191  $8.854 \times 10^{-12} \text{ Farad m}^{-1}$ , i.e.  $\epsilon_1$  is not considered as zero during all calculations.  
192 Under these conditions, the formula listed above are still suitable and more  
193 explanations about the potential formulation of a horizontal electric dipole can be  
194 found in the Appendix A of Key (2009) and related programs are available with an  
195 access to the website (<http://marineemlab.ucsd.edu/>). The horizontal finite length  
196 dipole source can be **viewed** as integral of an infinite small horizontal dipole during  
197 related calculations.

198

### 199 **3 Simulation results**

200 According to these two models **presented** above, several free parameters must be  
201 specified in order to investigate the attenuation characteristics of the electromagnetic  
202 fields emitted by a long x-directed dipole current source. As for the parameters of the  
203 dipole current source, we select  $L=150 \text{ km}$ , the Wenchuan earthquake main rupture  
204 stage within 30 s out of 90 s ( $\sim 300 \text{ km}$ ) based on Zhang et al., (2009, Fig.1), the

205 depth  $d = 19$  km (Xu, 2009), the hypocenter depth of the Wenchuan case and the  
 206 current is set to be  $I=1$  A temporarily. Here, the Earth is considered to be an isotropic  
 207 media with an average conductivity  $\sigma_1$ , and we assume  $\sigma_1 = 1.0 \times 10^{-3} \text{ S m}^{-1}$  at  
 208 this time, i.e.  $\rho_1 = 10^3 \text{ ohm} \cdot \text{m}$ , although the ground conductivity depends not only  
 209 on the local petrology, but also on the porosity, temperature, and pressure (e.g., Wait,  
 210 1966). All these parameters are common to two models. The parameter  $\epsilon_{-1} = 5\epsilon_0$  is  
 211 of most importance during the calculation in three-layer model in that it potentially  
 212 can affect the transmission of electromagnetic waves produced by the dipole beneath  
 213 the Earth, and possibly induce the Earth-atmosphere-ionosphere electromagnetic  
 214 coupling.



231 **Fig.2.** Electric field  $|E_x|$  decay curves along x-axial direction as a function of the observing  
 232 distance for the Cartesian coordinate system with different frequencies. Red solid lines stand for  
 233 electric field curves for Earth-air model and blue dot lines denote electric field curves with the  
 234 ionospheric effect for Earth-air-ionosphere model.

- 235 (a) Total  $|E_x|$  for  $f=0.01$  Hz; (b) Total  $|E_x|$  for  $f=0.1$  Hz;  
 236 (c) Total  $|E_x|$  for  $f=1$  Hz; (d) Total  $|E_x|$  for  $f=10$  Hz;

237  
 238 Fig.2a-d displays electric field amplitude  $|E_x|$  decay curves along the x-axial



239 direction with the frequencies  $f=0.01$  Hz,  $f=0.1$  Hz,  $f=1$  Hz, and  $f=10$  Hz respectively  
240 for the Cartesian coordinate system up to  $\sim 10,000$  km on the Earth's surface.

241 It can be seen from Fig.2a-d, first, the electrical field with "high" frequency has a  
242 big attenuation although all curves for both Earth-air model (red solid lines) and  
243 Earth-air-ionosphere model (blue dot lines) decay rapidly as the distance increases.  
244 Second, each group of curves run at the same level for one fixed frequency, e.g.,  $f=1$   
245 Hz, when an observing point is located at a relative near distance,  $\sim 300$  km for  $f=1$   
246 Hz (Fig.2c) for example. That is to say, the ionospheric influence on electromagnetic  
247 field transmissions can be neglected within this range. However this range changes  
248 for different frequencies and it becomes smaller as the operating frequency of the  
249 current source increases (e.g., more than 1000 km for  $f=0.01$  Hz (Fig.2a) and only  
250  $\sim 200$  km for  $f=10$  Hz (Fig.2d)). Third, the most important result is, as the distance  
251 increases, field curves with an ionospheric effect (blue dot lines) run **along** a different  
252 **path** from that of curves without an ionospheric effect (red solid lines) and the  
253 ionospheric lines attenuate more slowly. Now, this kind of ionospheric influence can  
254 no longer be neglected. The ionospheric difference is about 1 magnitude ( $\times 10$ ) for all  
255 the frequencies listed and even once up to 2 magnitudes for  $f=10$  Hz within the range  
256 shown in Fig.2. For example, the ionospheric difference value shows 1 magnitude  
257 from  $\sim 840$  km, up to 2 magnitudes from  $\sim 3,700$  km for  $f=10$  Hz (Fig.2d).

258

## 259 **4 The Wenchuan $M_S=8.0$ earthquake as a sample**

### 260 **4.1 Estimating the seismo-telluric current magnitude**

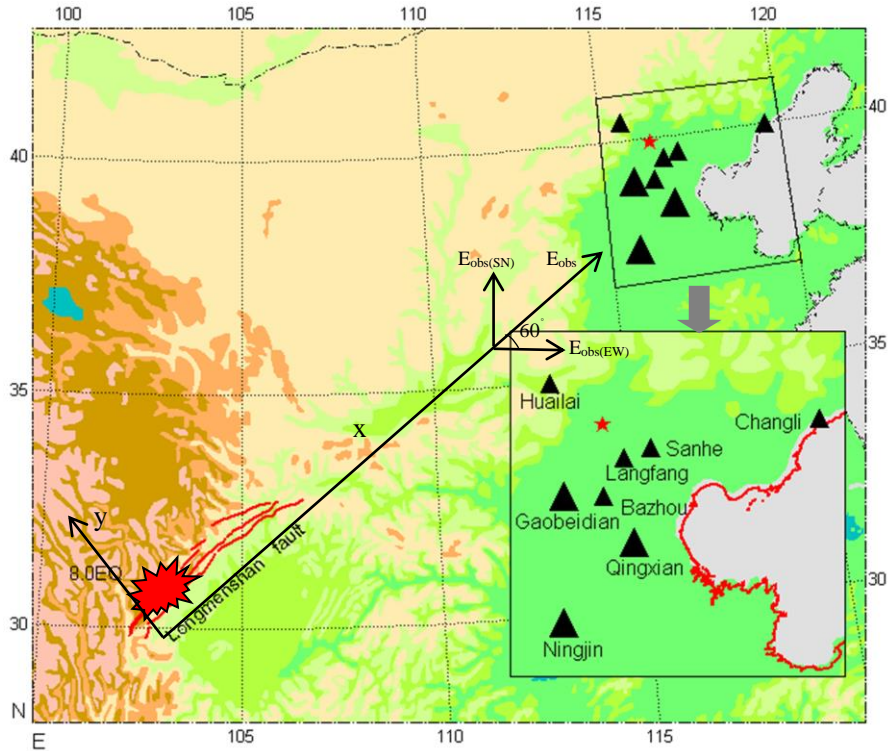
261 On the base of the work of rock experiments conducted under laboratory  
262 conditions, there is a reason to believe that a giant seismo-telluric current is generated  
263 when the main rupture took place during the Wenchuan earthquake on 12 May 2008  
264 and that this current mainly **propagated** along the Longmenshan fault. At the same  
265 time a strong electrical field induced by this current suddenly increased. This  
266 electrical field was recorded at the ground-based Gaobeidian ULF observing station,  
267 1440 km away from the epicenter of the shock, with a SN (**South-North**) maximum  
268 amplitude of 70 mm, i.e.  $1.3 \text{ mV m}^{-1}$  (Li et al., 2013), that is  $E_{\text{obs(SN)}} = 1.3 \text{ mV m}^{-1}$  in  
269 the following statement (Fig. 3).

270

271



272  
273  
274  
275  
276  
277  
278  
279  
280  
281  
282  
283  
284  
285  
286



287 **Fig.3.** Distribution of the Wenchuan earthquake epicenter and observation stations. Black solid  
288 triangles present the related locations of observation stations in Hebei electromagnetic observation  
289 network, bigger ones indicate the stations where abnormal information was recorded and the red  
290 star denotes Beijing (Li et al., 2013, Fig.1). A ground surface coordinate system is added.

291

292 In order to establish a relationship between the seismo-telluric current during the  
293 main event and the observable ground electrical signals registered at Gaobeidian  
294 station, we consider that a finite length current dipole source, with the length being  
295 the main rupture  $L=150$  km of the Wenchuan earthquake and the current  $I$ , is  
296 co-located with the Longmenshan main fault (x-direction), with the depth being  $d=19$   
297 km. Then one can refer to Fig.1 with ionospheric effect.

298 **Corresponding to Fig.1,** a coordinate system on the Earth's surface (see Fig.3) is  
299 set up to calculate the observable electrical field along the x-direction  $E_{obs}$  according  
300 to the electrical value  $E_{obs(SN)}=1.3$  mV m<sup>-1</sup> recorded at the Gaobeidian station. The  
301 Gaobeidian station lies in the extended line of the Longmenshan fault, which trends  
302 northeast and dips about 60° west (Xu, 2009). Other locations of stations are shown in  
303 Fig.1 of Li et al. (2013) and here they are shown in Fig.3 which includes a ground  
304 surface coordinate system. From Fig.3, we see that the electrical field component  
305 intensity along the x-direction is about  $|E_x|=E_{obs}=1.5$  mV m<sup>-1</sup> ( $E_{obs(SN)}=\sin 60^\circ \times$

306  $E_{\text{obs}}=1.3 \text{ mV m}^{-1} \rightarrow E_{\text{obs}}=1.5 \text{ mV m}^{-1}$ ).

307 As the observing frequency of the electromagnetic observation system is 0.1-10  
308 Hz and the recorder belongs to a real-time analog record, it is not easy to figure out  
309 the right frequency of the signals registered at the Gaobeidian station during the  
310 maximum stage prior to the Wenchuan earthquake. We set the main frequency  $f=1$  Hz  
311 during our calculations although the information is of a short period  $\sim 0.1-0.3$  s and a  
312 large amplitude  $\sim 1.3 \text{ mV m}^{-1}$  (Li et al., 2013) and frequency bands (0.4-3 s and  
313 0.05-0.1 s) with various amplitudes were observed (Guan et al., 2003). At the same  
314 time, the results of 2D MT inversion in the Longmenshan fault show that the apparent  
315 resistivity logarithm is  $\sim 1-4.8$  (Zhu et al., 2008) and it is a wide range.

316

317

318

319

320

321

322

323

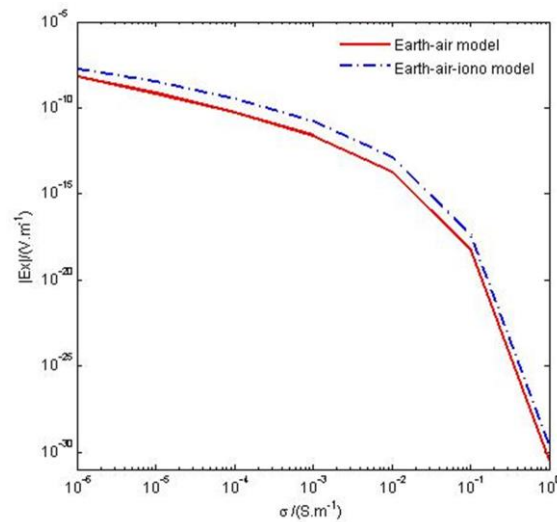
324

325

326

327

328



329

329 **Fig.4.** The calculated value of  $|E_x|$ , expected at the observation location (1,440 km, 0, 0) due to a  
330 dipole source of  $L=150$  km,  $I=1$  A,  $f=1$  Hz and  $d=19$  km (Fig.1), as a function of the typical  
331 crustal materials conductivity  $\sigma$  both in Earth-air model (red line) and in Earth-air-ionosphere  
332 model (blue dot line).

333

334 Fig. 4 shows the calculated values of  $|E_x|$ , expected at the observation location  
335 (1,440 km, 0, 0) due to a dipole source of  $L=150$  km,  $I=1$  A and  $d=19$  km (Fig.1), as a  
336 function of the typical crustal materials conductivity  $\sigma$ . Comparing with the red line  
337 with the blue dot one, the ionospheric effect is clearly displayed throughout the  
338 variation of the crustal conductivity. A rapid attenuation (in excess of 20 of magnitude)  
339 of the field values indicates the importance of the conductivity  $\sigma$ . It is difficult to

340 specify the average conductivity  $\sigma$  (referred to as  $\sigma_1$  in the context) of the  
341 homogeneous Earth medium, even for the typical Wenchuan area. However,  
342 combined with  $f=1$  Hz here, the skin-depth depends on the conductivity  $\sigma$ , given by  
343 the formula  $\delta = (\pi f \mu_0 \sigma)^{-\frac{1}{2}}$ . Taken the depth  $d=19$  km into account, here  $\delta = d =$   
344 19 km and the calculated  $\sigma_1$  is attained, i.e.  $\sigma_1 = 7.0 \times 10^{-4} \text{ S m}^{-1}$ , which is  
345 advantageous to radiate electromagnetic waves within this depth.

346 Using the same parameters as above, the simulation results show that the  
347 seismo-telluric current along the main fault needed to produce an electrical ground  
348 signal  $E_{\text{obs(SN)}} = 1.3 \text{ mV m}^{-1}$  at the Gaobeidian station when the Wenchuan event  
349 occurred, is about  $5.3 \times 10^7 \text{ A}$  with the ionospheric effect and  $3.7 \times 10^8 \text{ kA}$  without the  
350 ionospheric effect. As it is expected, these two results have one magnitude ( $\times 10$ )  
351 difference from each other. While the former is more reasonable under this conditions  
352 because the seismo-telluric current produced by the Wenchuan main rupture is  
353 specified.

354

#### 355 **4.2. Detectability under the ionospheric effect**

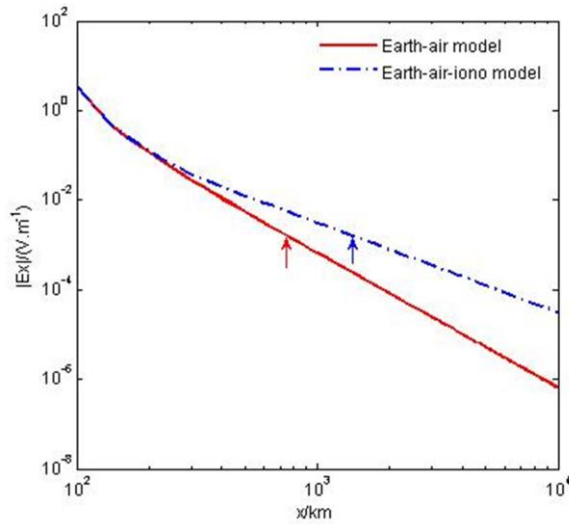
356 Now according to the Wenchuan earthquake example, the seismo-telluric current  
357 source ( $f=1$  Hz,  $d = 19$  km,  $L=150$  km, and a current  $I=5.3 \times 10^7 \text{ A}$  considering the  
358 Earth-air-ionosphere model) is thought of as a powerful finite length dipole source.

359 Fig.5 displays the fluctuations of the surface electrical fields with and without  
360 ionospheric effect for the Wenchuan source along x-axial direction. It shows no  
361 obvious ionospheric effect within 300 km, while this effect is roughly up to 1 **order of**  
362 magnitude from  $\sim 800$  km. The gap becomes larger as the distance **increases**, 2  
363 magnitudes from  $\sim 4000$  km, and then it keeps this gap till 10,000 km. Under this  
364 condition, considering the observable signal  $1.5 \text{ mV m}^{-1}$  at Gaobeidian station before  
365 the Wenchuan epicenter, the distance recorded such a signal must be  $\sim 1500$  km  
366 (blue arrow) with ionospheric effect, or it is only  $\sim 800$  km (red arrow) without  
367 ionospheric effect. So the ionosphere facilitates the electromagnetic wave propagation,  
368 as if the detectability of the system **were** improved effectively and it **would be** easier  
369 to record a signal even **at** stations located beyond their detectability threshold.

370

371

372  
373  
374  
375  
376  
377  
378  
379  
380  
381  
382  
383



384 **Fig.5.** The Wenchuan source producing electric field  $|E_x|$  decay curves as a function of the  
385 distance along x-axial direction with ionospheric effect (blue dot line), as well as without  
386 ionospheric effect (red line). The electric field  $|E_x|=1.5 \text{ mV m}^{-1}$  is labeled by a red arrow and a  
387 blue one respectively.

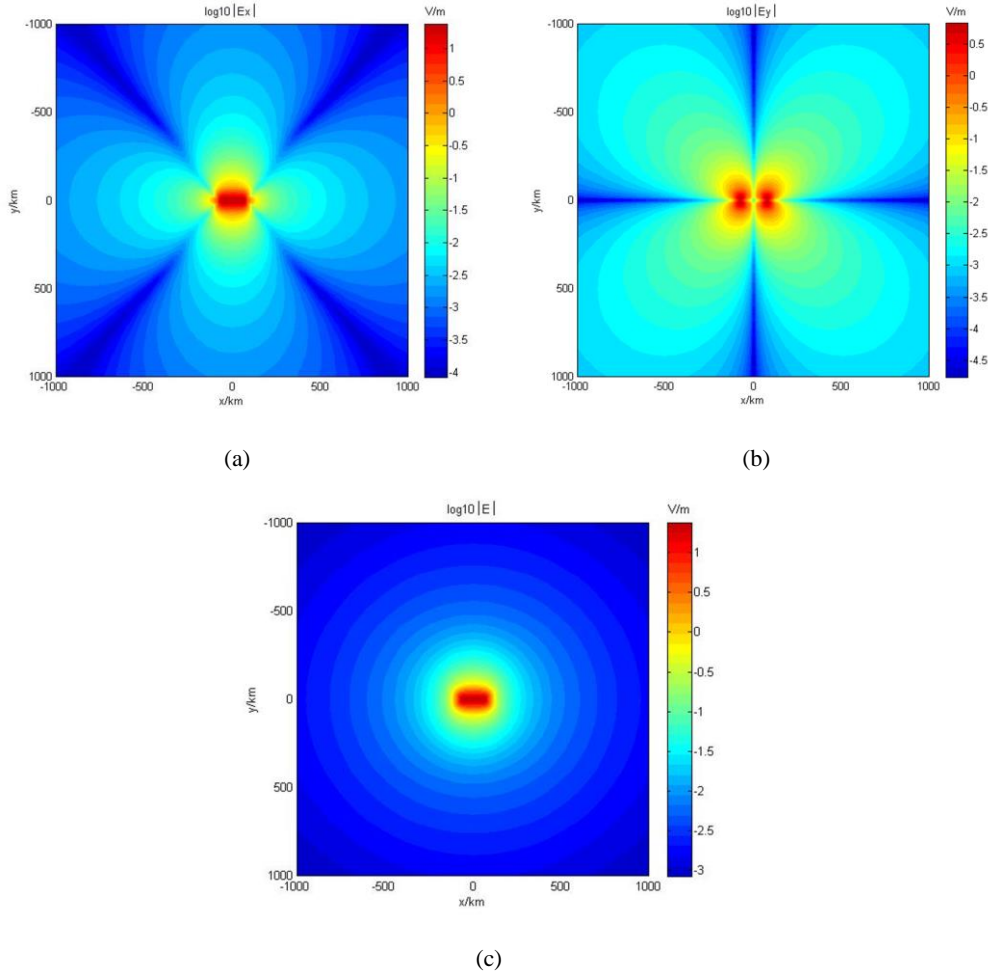
388  
389

### 4.3. Wave 2-D distribution

390 We perform electromagnetic wave fields for the Wenchuan source and this is  
391 done in the ground plane region  $-1,000 \text{ km} < x < 1,000 \text{ km}$  and  $-1,000 \text{ km} < y < 1,000 \text{ km}$   
392 in order to visualize the 2-D distribution of the wave power surrounding the electrical  
393 source.

394 Figure 6 displays the 2-D power distributions of the electrical field components  
395  $|E_x|$ ,  $|E_y|$  and the total  $|E|$  ( $|E|^2 = |E_x|^2 + |E_y|^2$ ) after making a logarithm calculation on  
396 the Earth's surface. It can be seen firstly from Figure 6a that there is an obvious  
397 constant strong power along the current element length ( $-75 \text{ km} < x < 75 \text{ km}$ ) in the  
398 x-direction. The electrical value in this area is not discussed here because it is usually  
399 considered not precise. Then the strong field radiates outward surrounding four main  
400 axes, indicating 1 order rough decay of the field at  $\sim 160 \text{ km}$ , 2 orders of magnitude  
401 at  $\sim 320 \text{ km}$  from the source endpoint in the x-direction. There is only 3 orders decay  
402 till 1,000 km away because of the ionospheric facilitating effect on the field and it  
403 keeps a strong value ( $\sim 1.86 \text{ mV}$ ) which can be fairly recorded by the stations.  
404 However, there are also weak power areas along lines, which form  $45^\circ$  angle with the  
405 principal axis for the electrical field power  $|E_x|$  (Figure 6a). Complementally, the  
406 electrical field power  $|E_y|$  (Figure 6b) is basically characterized by strong power areas

407 between two main axes, as well as weak ones along four chief axes. The power  
 408 distribution of the total  $|E|$  consequently presents to be symmetry to the center circle  
 409 outside of the source (Figure 6c), which also indicates that the radiating patterns of  
 410 the electrical field power  $|E_x|$  and the electrical field power  $|E_y|$  are complementary  
 411 (One is strong area and the other is weak area) each other surrounding the source.



437 **Fig.6.** 2-D distributions of electrical field power  $|E_x|$  (a),  $|E_y|$  (b) and total  $|E|$  (c) after a  
 438 logarithm calculation for the Wenchuan source using Earth-air-ionosphere model.

## 440 5 Discussion

441 In very recent years, there is an increasing amount of evidence that during some  
 442 last stages of the long term process of preparation, there could be a transfer of energy  
 443 between lithosphere and the above layers of atmosphere and ionosphere, so as to  
 444 introduce the concept of a lithosphere–atmosphere–ionosphere coupling (LAIC)  
 445 among the three involved layers of the Earth system (Pulinets et al., 2000; Hayakawa  
 446 and Molchanov, 2002; Molchanov et al., 2004; Pulinets and Ouzounov, 2011). On

447 one hand, the ‘energy source’ is usually thought to be beneath the Earth’s surface and  
448 related to tectonic activities in the lithosphere. On the other hand, numerous  
449 rock-pressure experiments and electromagnetic observations associated with seismic  
450 activities have already proved that a giant electrical current and an abrupt increase of  
451 electromagnetic signals occur during the main rupture of stressed-rocks. These  
452 phenomena happened on May 9 2008, 3 days before the Wenchuan event, which  
453 hypocenter lies in mid-crust. The strong seismo-telluric current is thought to run  
454 mainly along the Longmenshan fault and electromagnetic oscillations, induced by the  
455 current and predominated by ULF frequency band, propagate up to ionosphere and  
456 give rise to perturbations of ionospheric parameters. Some of these parameters have  
457 been investigated, such as GPS TEC and f0F2 (Yu et al., 2009; Xu et al., 2010;  
458 Akhoondzadeh et al., 2010), DEMETER satellite O+ density (Zhang et al., 2009),  
459 electron density and electron temperature (Zeng et al., 2009), and so on. Fortunately,  
460 all these study results present a climax on May 9 and this indicates a lithosphere–  
461 atmosphere–ionosphere coupling or interaction aroused by these electromagnetic  
462 signals prior to the Wenchuan event.

463 Unfortunately, at present, most of investigations put emphases on the effect of  
464 earthquakes upon the ionosphere and few of them pay attention to an inverse problem,  
465 that is the ionospheric influence on the electromagnetic waves passing through.

466 The ionosphere, as a part of the electrical conducting region of the upper  
467 atmosphere, can enhance electromagnetic fields and cause the decay as a function of  
468 distance to slow down when an observation is within ionospheric range and the  
469 ionospheric effect can be up to 1-2 magnitudes of the electrical fields in our simply  
470 three-layer model for some specified parameters we have selected here.

471 Considering the Wenchuan event, the electrical signals from the lithosphere  
472 interact with the ionosphere and are at the same time enhanced, and then registered at  
473 1440km Gaobeidian station with the amplitude of  $1.3 \text{ mV m}^{-1}$ . This electrical field is  
474 used to simulate the seismo-telluric current produced by the Wenchuan main rupture  
475 in an Earth-air-ionosphere model together with an Earth-air model. The results present  
476 that, the seismo-telluric currents with and without ionospheric effect must be about  
477  $5.3 \times 10^7 \text{ A}$  and  $3.7 \times 10^8 \text{ A}$  respectively. Compared with the expected seismo-telluric  
478 current  $\sim 10\text{--}100 \text{ kA}$  of the “Alum Rock”  $M_w=5.6$  earthquake for an observed 30 nT  
479 pulse at 1 Hz and  $D=2 \text{ km}$  (Bortnik et al., 2010), this result is probably in a reasonable  
480 range.



481 However, firstly, the total rupture of the Longmenshan fault during the  
482 Wenchuan main shock is extremely complicated that comprises of tenths of rupture  
483 stages and several pauses, totaling 90 s for the whole rupture process ( $\sim 300$  km),  
484 according to Zhang et al.,(2009). Thus the total surface rupture  $\sim 300$  km is  
485 nevertheless not used here. While performing the analysis on only the primary 30 s, a  
486 main stage of the Wenchuan earthquake, out of 90 s as we have selected  $L=150$  km  
487 above, is expected to be representative of the majority of the rupture to generate a  
488 seismo-telluric current. Secondly, three medium are thought of as a homogeneous  
489 isotropic medium in our models and with the same average conductivity value for  
490 each one, especially for the wenchuan area. However, the Earth conductivity plays  
491 such an important role that it predominately affects the fluctuations of the electrical  
492 fields as shown in Fig.4 although no one exactly knows the right conductivity of the  
493 Earth medium at the rupture depth. The value  $\sigma_1 = 7.0 \times 10^{-4} \text{ S m}^{-1}$  taken part in  
494 all analysis is estimated when the observing frequency range  $f=0.1-10$  Hz and the  
495 hypocenter depth  $d=19$  km of the Wenchuan main event are taken into account for the  
496 skin-depth formula. One must also mention that we use  $f=1$  Hz in our calculations  
497 because we cannot identify the actual frequencies in the recorded analog signals. All  
498 these can underscore our simulation results.

499 While these disadvantageous selections maybe are not so important at the same  
500 time because the key point of this paper is of the ionospheric influence on  
501 electromagnetic wave propagation and our investigation attains advantageous results.

502 The “selectivity” or “orientation” of the electromagnetic information is a very  
503 important character during seismic activities (Varotsos and Lazaridou, 1991). For a  
504 finite length dipole source of the Wenchuan earthquake, its 2-D distributions of  
505 electrical field component  $|E_x|$  and  $|E_y|$ , which are orthogonal each other, on the  
506 Earth’s surface shows there are strong field power areas and weak field power areas  
507 around the source as illustrated by [Bortnik et al., 2010]. While the radiating pattern  
508 of the total  $|E|$  in this investigation is symmetry to the center circle outside of the  
509 source which indicates a signal is always registered to anyone direction if a system is  
510 designed to measure the total field  $|E|$  or both of  $|E_x|$  and  $|E_y|$  components instead of  
511 only one. This result also basically supports the practices of “selectivity” or  
512 “orientation”, the observing reality before the Wenchuan earthquake described by Li  
513 et al.[2013], for example, ‘Compared with the EW (East-West) orientation, the  
514 electromagnetic signal is more obvious in the SN (South-North) orientation’. The



515 selectivity effect is a complex phenomenon that may be attributed to a superposition  
516 of the following three factors: “source characteristics”, “travel path” and  
517 “inhomogeneities close to the station” [Varotsos and Lazaridou, 1991; Varotsos et al.,  
518 2005]. Analytical solutions of Maxwell equations [Varotsos et al., 2000], as well as  
519 numerical ones [Sarlis et al., 1999], convince that selectivity results from the fact that  
520 earthquakes occur by slip on faults which are appreciably more conductive than the  
521 surrounding medium.

522

## 523 **6 Conclusions**

524 In this paper, a three-layer (Earth-air-ionosphere) physical model, as well as a  
525 two-layer (Earth-air) model, is employed to investigate the ionospheric effect on the  
526 wave fields for a finite length dipole current source co-located with the main fault of  
527 an earthquake when an observing location distance is up to one thousand kilometers  
528 or even more. For a dipole source with specified parameters of the length  $L=150$  km,  
529 the current  $I=1$  A, and the depth  $d=19$  km, the results show that all fields are free of  
530 the ionospheric effect for different frequencies in relative short ranges, e.g.,  $\sim 600$   
531 km for  $f=0.1$  Hz, which implies the ionospheric influence on electromagnetic field  
532 transmissions can be neglected within this range. However, the ionosphere can  
533 increase the field amplitude and slow the decay when an observation is out of this  
534 range and the ionospheric effect can be up to 1-2 magnitudes of the electrical fields.

535 This is applicable to the 12 May 2008 Wenchuan  $M_S=8.0$  earthquake during  
536 which a strong electromagnetic signal with an amplitude of  $\sim 1.3$  mV m<sup>-1</sup>, is recorded  
537 by the Gaobeidian ULF ( $f=0.1-10$  Hz) observing station 1440 km from the epicenter.  
538 The main fault rupture producing a current is equivalent to a finite length dipole  
539 current source, with a nucleation depth of 19 km and a length of 150 km. Considering  
540 the Earth-air-ionosphere model, the expected current for the most typical properties of  
541 Wenchuan area is of  $5.3 \times 10^7$  A, which is of one magnitude smaller than the current  
542 value of  $3.7 \times 10^8$  A obtained with the Earth-air model free of ionospheric effect. On  
543 the contrary, a signal introduced by a seismic activity can be advantageously recorded  
544 by a remote station under the ionospheric effect as if the detectability of the system is  
545 improved effectively.

546 The 2-D power distributions of the electrical field component  $|E_x|$ ,  $|E_y|$  and the  
547 total  $|E|$  after making a logarithm calculation on the Earth's surface are characterized  
548 by different radiating patterns. There are strong power areas along four main axes as

549 well as weak power areas between two main axes for the electrical field  $|E_x|$ . While  
550 the component  $|E_y|$  displays a complementary radiating pattern with strong areas and  
551 weak areas. Therefore, fortunately, a signal is always registered to anyone direction if  
552 a system is designed to measure the total field  $|E|$  (or both  $|E_x|$  and  $|E_y|$  components)  
553 as the radiating pattern of which is Symmetry to the center circle outside of the  
554 source.

555

556 *Acknowledgements and data.* The authors are grateful to the National Natural Science  
557 Foundation of China and this work was sponsored by the project Simulation and  
558 Interpretation of the Spatial Electromagnetic Phenomena Coupling before the  
559 Wenchuan  $M_S8.0$  Earthquake under grant agreement n<sup>o</sup>41204057. The data presented  
560 in this paper are available to the e-mail: [limeixuxl@seis.ac.cn](mailto:limeixuxl@seis.ac.cn).

561

562 Edited by: C. Krawczyk

563 Reviewed by: F. Freund and ...

564

## 565 **References**

566 Akhoondzadeh, M., Parrot, M., and Saradjian M. R.: Electron and ion density  
567 variations before strong earthquakes ( $M>6.0$ ) using DEMETER and GPS data, Nat.  
568 Hazards Earth Syst. Sci., 10, 7–18, 2010.

569 Bernardi, A., Fraser-Smith, A. C., McGill, P. R., and Villard Jr, O. G.: Magnetic field  
570 measurements near the epicenter of the  $M_S7.1$  Loma Prieta earthquake, Phys. Earth  
571 Planet, Interiors, 68, 45–63, 1991.

572 Bortnik, J., Bleier, T. E., Dunson, C., and Freund, F., Estimating the seismo-telluric  
573 current required for observable electromagnetic ground signals, Ann. Geophys., 28,  
574 1615–1624, doi:10.5194/angeo-28-1615-2010, 2010.

575 Cummer, S.A.: Modeling Electromagnetic Propagation in the Earth-Ionosphere  
576 Waveguide, IEEE Transactions on Antennas and Propagation, 48(9), 2–12, 2000.

577 Draganov, A. B., Inan, U. S., and Taranenko, Y. N.: ULF magnetic signatures at the  
578 Earth due to groundwater flow: a possible precursor to earthquakes, Geophys. Res.  
579 Lett., 18, 1127–1130, 1991.

580 Eftaxias, K., Kaporis, P., Polygiannakis, J., Peratzakis, A., Kopanas, J., Antonopoulos,  
581 G., and Rigas D.: Experience of short-term earthquake precursors with VLF-VHF  
582 electromagnetic emissions, Nat. Hazards Earth Syst. Sci., 3, 217–228, 2002.

583 Egbert, G. D.: On the generation of ULF magnetic variations by conductivity  
584 fluctuations in a fault zone, Pure Appl. Geophys., 159, 1205–1227, 2002.

585 Fenoglio, M. A., Johnston, M. J. S., and Byerlee J. D.: Magnetic and electric fields  
586 associated with changes in high pore pressure in fault zones: application to the  
587 Loma Prieta ULF emissions, *J. Geophys. Res.*, 100 (12), 951–958, 1995.

588 Fraser-Smith, A. C., Bernardi, A., McGill, P. R., Ladd, M. E., Helliwell, R. A., and  
589 Villard Jr, O. G.: Low-frequency magnetic measurements near the epicenter of the  
590 *Ms* 7.1 Loma Prieta earthquake, *Geophys. Res. Lett.*, 17, 1465–1468, 1990.

591 Freund, F., and Sornette, D.: Electro-magnetic earthquake bursts and critical rupture  
592 of peroxy bond networks in rocks, *Tectonophysics*, 431, 33–47, 2007.

593 Freund, F., and Wengeler, H.: The infrared spectrum of OH<sup>-</sup> compensated defect sites  
594 in C-doped MgO and CaO single crystals. *J. Phys. Chem. Solids* 43, 129–145,  
595 1982.

596 Freund, F.: Charge generation and propagation in igneous rocks, *J. Geodynamics*, 33,  
597 543–570, 2002.

598 Freund, F.: Conversion of dissolved “water” into molecular hydrogen and peroxy  
599 linkages. *J. Non-Cryst. Solids* 71, 195–202, 1985.

600 Freund, F.: Stress-activated positive hole charge carriers in rocks and the generation  
601 of pre-earthquake signals, in: *Electromagnetic Phenomena Associated with*  
602 *Earthquakes*, edited by: Hayakawa, M., Transworld Research Network, Trivandrum,  
603 India, Chapter 3, 41–96, 2009.

604 Freund, F.: Toward a unified solid state theory for pre-earthquake signals, *Acta*  
605 *Geophys.*, 58(5), 719–766, 2010.

606 Fu, C. M., Di, Q. Y., Xu, C., and Wang, M. Y.: Electromagnetic fields for different  
607 type sources with effect of the ionosphere, *Chinese J. Geophys.*, 55(12), 3958–3968,  
608 doi: 10. 6038/ j. issn. 0001-5733. 2012. 12. 008, 2012(in Chinese with English  
609 abstract).

610 Guan, H. P., Han, F.Y., Xiao, W. J., and Chen, Z.Y.: ULF electromagnetic  
611 observation and data processing methods, *Earthquake*, 23(2), 5–93, 2003(in  
612 Chinese with English abstract).

613 Hayakawa, M., and Molchanov, O. A. (Eds.): *Seismo-Electromagnetics:*  
614 *Lithosphere-Atmosphere-Ionosphere Coupling*, p. 477. Tokyo, Japan:  
615 TERRAPUB , 2002.

616 Key, K.: 1D inversion of multicomponent, multi-frequency marine CSEM data:  
617 Methodology and synthetic studies for resolving thin resistive layers, *Geophysics*,  
618 74(2), F9–F20, 2009.

619 Kopytenko, Y. A., Matiashvili, T. G., Voronov, P. M., Kopytenko, E. A., and  
620 Molchanov, O. A.: Detection of ultra-low frequency emissions connected with the  
621 Spitak earthquake and its aftershock activity, based on geomagnetic pulsations data  
622 at Dusheti and Vardzia observatories, *Phys. Earth Planet. Interiors*, 77, 85–95,

623 1993.

624 Kuo, C. L., Huba, J. D., Joyce, G., and Lee, L. C.: Ionosphere plasma bubbles and  
625 density variations induced by pre-earthquake rock current and associated surface  
626 charges, *J. Geophys. Res.*, 116(10), A10317, doi:10.1029/2011JA016628, 2011.

627 Li, M., Lu, J., Parrot, M., Tan, H., and Zhang, X.: Review of unprecedented ULF  
628 electromagnetic anomalous emissions possibly related to the Wenchuan  $M_S = 8.0$   
629 earthquake, on 12 May 2008. *Nat. Hazards Earth Syst. Sci.*, 13(2), 279–286,  
630 doi: 10.5194/nhess-13-279-2013, 2013.

631 Li, D., Di, Q. Y., and Wang, M. Y.: One-dimensional electromagnetic fields forward  
632 modeling for “earth–ionosphere” mode. *Chinese J. Geophys.*, 54(9), 2375–2388,  
633 doi: 10.3969/j.issn.0001–5733.2011.09.021, 2011 (in Chinese with English  
634 abstract).

635 Li, Y., Lin, P. R., Zheng, C. J., Shi, F. S., Xu, B. L., and Guo, P.: The electromagnetic  
636 response modeling of the ELF method and the influence of the ionosphere,  
637 *Geophysical & Geochemical Exploration*, 34(3), 332–339, 2010a, (in Chinese with  
638 English abstract).

639 Li, D. Q., Di, Q. Y., and Wang, M. Y.: Study of large scale large power control source  
640 electromagnetic with “Earth–ionosphere” mode, *Chinese J. Geophys.*, 53(2), 411–  
641 420, doi: 10.3969/j.issn.0001-5733.2010.02.019, 2010b, (in Chinese with  
642 English abstract).

643 Molchanov, O. A., Kopytenko, Y. A., Voronov, P. M., Kopytenko, E. A., Matiashvili, T.  
644 G., Fraser-Smith, A. C., and Bernardi, A.: Results of ULF Magnetic field  
645 measurements near the epicenters of the Spitak ( $M_s$  6.9) and Loma Prieta ( $M_s$  7.1)  
646 earthquakes: comparative analysis, *Geophys. Res. Lett.*, 19, 1495–1498, 1992.

647 Molchanov, O. A., Fedorov, E., Schekotov, A., Gordeev, E., Chebrov, V., Surkov,  
648 V., ..., Biagi, P. F.: Lithosphere-atmosphere-ionosphere coupling as governing  
649 mechanism for preseismic short-term events in atmosphere and ionosphere, *Natural*  
650 *Hazards Earth Syst. Sci.*, 4, 757-767, 2004.

651 Ohta, K., Umeda, K., Watanabe, M. and Hayakawa, M.: Relationship between ELF  
652 magnetic field and Taiwan earthquake. In *Lithosphere-Atmosphere-Ionosphere*  
653 *Coupling* (eds M. Hayakawa and O. A. Molchanov), Terra Science Publishers,  
654 Tokyo, pp. 233–237, 2002.

655 Panfilov, A. A.: The results of experimental studies of VLF–ULF electromagnetic  
656 emission by rock samples due to mechanical action, *Nat. Hazards Earth Syst. Sci.*,  
657 14, 1383–1389, doi:10.5194/nhess-14-1383-2014, 2014.

658 Park, S. K.: Precursors to earthquakes: seismo-electromagnetic signals, *Surv.*  
659 *Geophys.*, 17, 493–516, 1996.

660 Pulinet, S. A., and Ouzounov, D.: Lithosphere-Atmosphere-Ionosphere Coupling

661 (LAIC) model-An unified concept for earthquake precursors validation, J.  
662 Southeast Asian Earth Sci., 41(4-5): 371-382, 2011.

663 Pulinets, S. A., Boyarchuk, K. A., Hegai, V. V., Kim, V. P., and Lomonosov, A. M.:  
664 Quasielectrostatic model of atmosphere-thermosphere-ionosphere coupling, Adv.  
665 Space Res., 26, 1209-1218, 2000.

666 Qian, S., Hao, J., Zhou, J. and Gao, J.: Precursory Electric and Magnetic Signals at  
667 ULF and LF Bands during the Fracture of Rocks under Pressure. Earthquake  
668 Research in China, 19(2), 109-116, 2003 (in Chinese with English abstract).

669 Qian, S., Hao, J., Zhou, J. and Gao, J.: Simulating experimental study on ULF  
670 electromagnetic precursors before Jiji Ms = 7.4 earthquake. In  
671 Lithosphere-Atmosphere-Ionosphere Coupling (eds Hayakawa, M. and Molchanov,  
672 O. A.), Terra Science Publishers, Tokyo, pp. 49-53, 2002.

673 Qian, S., Ren K., Lü, Z.: Experimental study on VLF, MF, HF and VHF  
674 electromagnetic radiation characteristics with the rock breaking, Earthquake  
675 Science, 18(3), 346-351, 1996 (in Chinese with English abstract).

676 Sarlis, N., Lazaridou, M., Kapiris, P., and Varotsos, P.: Numerical model of the  
677 selectivity effect and the V/L criterion, Geophys. Res. Lett., 26, 3245-3248, 1999.

678 Scoville, J., J. Sornette, and Freund, F. T.: "Paradox of peroxy defects and positive  
679 holes in rocks Part II: Outflow of electric currents from stressed rocks." Journal of  
680 Asian Earth Sciences 114, Part 2: 338-351, 2015.

681 Simpson, J. J., and Taflove, A.: Electrokinetic effect of the Loma Prieta earthquake  
682 calculated by an entire-Earth FDTD solution of Maxwell's equations. Geophys. Res.  
683 Lett., 32, L09302, doi: 10. 1029/2005GL022601, 2005.

684 Uyeda, S., Nagao, T., Orihara, Y., Yamaguchi, T., and Takahashi I.: Geoelectric  
685 potential changes: Possible precursors to earthquakes in Japan, Proc. Nat. Acad.  
686 Sci., 97, 4561-4566, 2000.

687 Varotsos, P., and Lazaridou, M.: Latest aspects of earthquake prediction in Greece  
688 based on seismic electric signals. Tectonophysics, 188, 321-347,1991.

689 Varotsos, P., Sarlis, N., and Lazaridou, M.: Transmission of stress induced electric  
690 signals in dielectric media, Part II, Acta Geophys, 48, 141-177, 2000.

691 Varotsos, P., Sarlis, N., Skordas, E., Tanaka, H., and Lazaridou, M.: Additional  
692 evidence on some relationship between seismic electric signals and earthquake  
693 source parameters, Acta Geophys., 53, 293-298, 2005.

694 Wait, J. R.: Geo-electromagnetism: Academic Press,1982.

695 Wait, J. R.: Some Factors Concerning Electromagnetic Wave Propagation in the  
696 Earth's Crust, Proc. IEEE, 54(8), August 1966.

697 Xu, C., Di, Q. Y., Fu, C. M. and Wang, M. Y.: The contrast of response  
698 characteristics between large power long dipole and circle source, Chinese J.

699 Geophys, 55(6), 2097–2104, doi: 10. 6038/ j. issn. 0001–5733. 2012. 06. 03, 2012,  
700 (in Chinese with English abstract).

701 Xu, T., Hu, Y., Wu, J., Wu, Z., Suo, Y., and Feng, J.: Giant disturbance in the  
702 ionospheric F2 region prior to the *M*8.0 Wenchuan earthquake on 12 May 2008,  
703 Ann. Geophys., 28, 1533–1538, 2010.

704 Xu, X. W.:Album of 5.12 Wenchuan 8.0 earthquake surface ruptures. Seismological  
705 press, 2009 (in Chinese with English abstract).

706 Yamauchi, T., Maekawa, S., Horie, T., Hayakawa, M., and Soloviev, O.:  
707 Subionospheric VLF/LF monitoring of ionospheric perturbations for the 2004  
708 Mid-Niigata earthquake and their structure and dynamics, J. Atmos. Sol. Terr.  
709 Phys., 69, 793–802, 2007.

710 Yu, T., Mao, T., Wang, Y. G., and Wang, J. S.: Study of the ionospheric anomaly  
711 before the Wenchuan earthquake, Chinese Science Bulletin, 54(6): 1086–1092, doi:  
712 10.1007/s11434-008-0587-8, 2009 (in Chinese with English abstract).

713 Zeng, Z. C., Zhang, B., Fang, G. Y., Wang, D. F., and Yin, H. J.: The analysis of  
714 ionospheric variations before Wenchuan earthquake with DEMETER data, Chinese  
715 J. Geophys., 52(1): 11–19, 2009 (in Chinese with English abstract).

716 Zhang, X., Shen, X., Liu, J., Ouyang, X., Qian, J., and Zhao, S.: Analysis of  
717 ionospheric plasma perturbations before Wenchuan earthquake. Nat. Hazards Earth  
718 Syst. Sci., 9: 1259–1266, 2009.

719 Zhang ,Y., Feng, W. P., Xu, L. S., Zhou, C. H., and Chen, Y. T.: Spatio-temporal  
720 rupture process of the 2008 great Wenchuan earthquake, Science in China Series D:  
721 Earth Sciences, 52 (2), 145–154, 2009.

722 Zhu, Y. T., Wang, X. B., Yu, N., Gao, S. Q., Li, K., and Shi, Y. J.: Longmenshan  
723 magnetotelluric deep structure and the Wenchuan earthquake (*M*<sub>S</sub>8.0), Acta  
724 Geologica Sinica, 82 (12), 1769–777, 2008 (in Chinese with English abstract).

725